In Situ Observation Of Multiple Failure Modes in a Cross-Ply Laminated Composite Structure Using 3D Micro-Computed Tomography with a DVC technique

Sooyoung Lee[1], Eonyeon Jo[2] and Wooseok Ji[3]
Ulsan National Institute of Science and Technology, Ulsan, S. Korea

In situ mechanical tests on a unidirectional fiber-reinforced composite material has been performed. Single-edge notched specimen with the layup sequence of $[90_2/0_2]_S$ was utilized for to observe subsurface damage and failure progression under tensile loading. Special loading frame was designed and fabricated for the in situ tests at a synchrotron facility. Three-dimensional tomography images show multiple failure modes occurring sequentially as the applied load increases. In the present study, the interactive failure mechanism under the surface of the composite materials has been revealed. DVC technique is also applied for the quantitative deformation analysis of the internal mechanical behavior.

I. Introduction

The present study is concerned with unique testing and visualization techniques to characterize complex and interacting failure modes observed in fiber-reinforced polymer (FRP) composites under mechanical loading. Composite structures are increasingly used in commercial and military aerospace applications owing to their specific weight advantages. However, due to the unique microstructure of the materials, composite structures suffer micro-damage and failure at the fiber length scale mainly because of the significant stiffness mismatch between a fiber and polymer matrix. Therefore, detailed physics of damage progression and failure mechanisms at the micro-length scale in composite materials should be carefully characterized since homogenized manifestations of the micro-scale deficiencies will be coupled to the higher length scales that may lead to catastrophic failure of an entire structural system. Although many researches have been performed to characterize damage and failure at the micro-length scale, they rely on hypothetical theories based on the observation of failure patterns from tested specimens. Detailed processes that lead to the final failure pattern are extremely difficult to obtain without a special testing instrument equipped with a microscopic device. **Digital image correlation (DIC) technique is now widely used to investigate the progressive damage and failure response of composite materials, but the information obtained from DIC is limited to surfaces where speckle patterns are applied**.

With the increasing interest in microscale experiments and the development of computational tomography resources, three-dimensional (3D) X-ray micro-computed tomography (μCT) has been utilized recently to visualize microstructural behavior in composite materials [1-8]. In the present study, we have developed an experimental technique that is capable of characterizing and quantifying damage progression and failure at micro-scale in a fully 3D setting. We have designed and built a micro tester that is driven by an electric servo motor and installed with a load cell. This tester is specially designed to be mounted on the synchrotron X-ray microscope facility at Pohang Accelerator Laboratory (PAL). We have performed experiments on composites specimens at the PAL on beamline 6C where the micro tester can be set up for in situ testing. This beamline 6C is equipped with various X-ray detectors with the FOV of 7 cm × 7 cm, 6 cm × 4 cm and less than 7 mm × 5 mm. The resolutions are 48, 32, 1-5 microns, respectively [9].

In the preset study, we have performed in situ mechanical testing on a single edge notched specimen with the stacking sequence of $[90_2/0_2]_S$. The specimen under tension exhibits various failure modes including microdamge due to matrix microcracking, intralaminar fracture modes and delamination. 3D tomography images obtained from the in situ tests clearly show the multiple failure patterns and their interaction.

---

[1] Graduate Student Research Assistant, Department of Mechanical Engineering, 50 Unist-gil, Ulju-gun.
[2] Graduate Student Research Assistant, Department of Mechanical Engineering, 50 Unist-gil, Ulju-gun.
[3] Assistant Professor, Department of Mechanical Engineering, 50 Unist-gil, Ulju-gun, Meber of AIAA.

II. Experimental Study

A. Design and fabrication of an in situ loading device

A special load frame for performing in situ mechanical tests in an X-ray synchrotron beamline was designed and fabricated. The loading device was designed such that it can be mounted on a high precision rotation stage that is installed in the X-ray tomography beamline (Beamline 6C) at PAL. In order to precisely control an elaborate movement of the rotation stage, the weight of our loading device did not exceed 20 kg, which is required by the specification of the precision stage. In addition, the height of the loading device was determined by accounting for the focal position of the X-ray beam when the device was placed on the optical table in the Beamline 6C. As a result, a small-scale loading frame was designed and fabricated as shown in Figure 1.

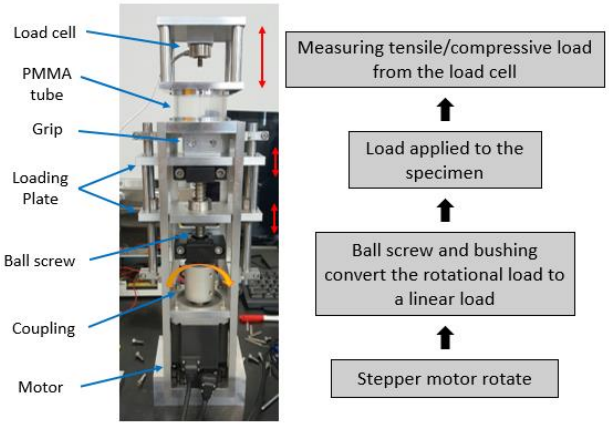

Figure 1: Overview of the in situ mechanical loading frame

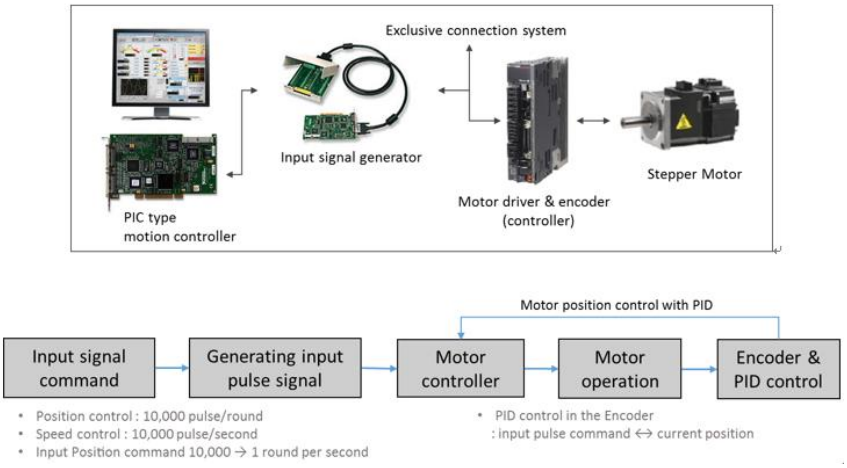

Figure 2: PID-based loading control system

Specimens were held between grips connected to a motorized loading fixture that applied loading to the samples in tension or compression. Motor control system was constructed to apply a specific loading rate to a specimen. Figure 2 schematically shows the control system. The loading control system consisted of a PCI-type motion controller, an input signal generator and a motor driver to precisely control a desired loading rate. When a specific loading rate was determined by a user, a pulse signal was generated from the generator for an input command to the motor. Then the motor driver in Figure 2 received the input signal and operated the motor. A ball screw and busing parts convert rotational energy from stepper motor to linear loading force on the specimen. Axial displacement due to the rotation of the motor shaft was measured by a high-resolution encoder (4M pulses/rev). By multiplying the number of rotations and pitch of the ball screw, the axial displacement was obtained. The motion controller based on the PID controller carried out a feedback control on the motor to achieve the specific loading rate given in axial displacement per minute. Applied load to the specimen was measured through a piezo-electric type load cell that was installed in the top part of the device as shown in Figure 1.

B. Test specimens for in situ experiments with X-ray tomography

Prepreg with a material system of UIN150/H15 was used to manufacture specimens for in situ experiments. Basic material properties of the prepreg is listed in Table 1. Single-edge notched specimens with a stacking sequence of $[90_2/0_2]_S$ were tested to closely investigate the interaction of multiple failure modes near the notch tip. Notches were carefully carved to avoid any undesirable initial damage such as delamination and bur that may affect in situ test results. Delamination and bur are typically observed when conventional working tools such as drill machine and router are used. In order to minimize initial damage to the specimen yet fabricate a very sharp notch, we utilized micro-resolution waterjet. The nozzle size of the waterjet was 0.35 mm, sufficient for fabricating sharp notches. Detailed dimensions of notches for the specimen can be found in Figure 3.

Properties	E_L (GPa)	E_T (GPA)	ν_{LT}	G_{LT} (GPa)	X_T (MPa)	Y_T (MPa)	S (MPa)
Values	146.45	7.439	0.34	4.15	2672	26.3	43.8

Table 1: Fundamental mechanical properties of the UIN150/H15 material system

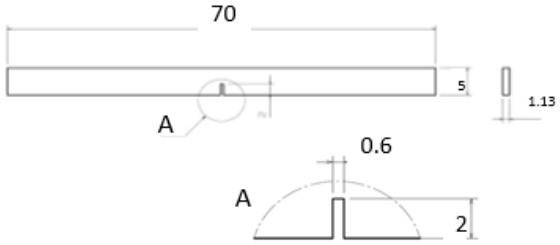

Figure 3: Dimensions of the specimen for the in situ testing (unit: millimeters)

C. In situ experiments using a synchrotron light source

The synchrotron light source has the highest power and thus is suitable to obtain high quality images. At Pohang Accelerator Laboratory (PAL), tension tests on the single edge notched specimens were performed using the in situ mechanical loading device. Figure 4(a) shows the custom-built loading device mounted on the precision rotation/translation stages in Beamline 6C at PAL. For the in situ mechanical testing, the first and the most important step is the beam alignment to place the specimen with respect to the beam path as shown in Figure 4 (b). At first, the *z*-direction positioning was carried out. The accurate beam line height was known and the position of the specimen was arranged to set the beam pass through its center. After the *z*-axis setup, the center of the beam path and the rotating axis of the loading device were aligned to reduce any potential noise factor. Since the rotation axis arrangement directly affects the quality of reconstructed 3D images, the process was carefully conducted. The arrangement was checked by comparing images taken at 0 degree and 90 degrees. Finally, the focusing process of the CCD camera shown in Figure 4(b) was conducted. The position of the focal point was decided on the desired magnification level. For the SENT test, we used 20× lens that resulted in the resolution of 0.45 micro-meter per pixel with the field of view (FOV) being 1.8 mm by 1.2 mm, which is fine and large enough to observe the initiation and propagation of cracks near the notch tip. X-ray images were taken at the nine loading steps as indicated in Figure 5. Displacement-controlled loading was applied to the specimen and a specific displacement was maintained while X-ray images were being taken at each of the nine steps.

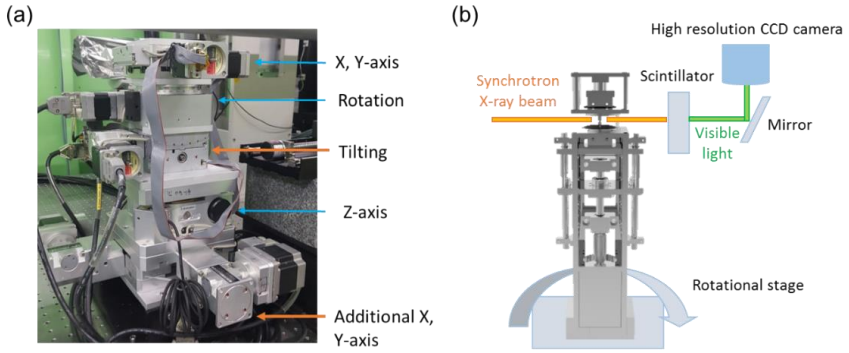

Figure 4: (a) Precision rotational/translational stages for the alignment of the specimen to the X-ray beam (b) Schematic illustration of the synchrotron X-ray beam system

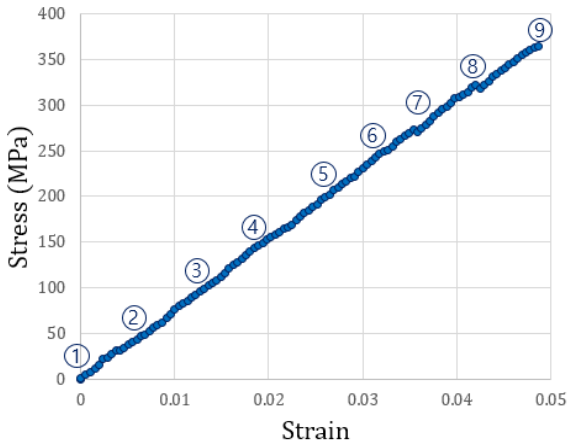

Figure 5: Stress-strain response of the SENT specimen. Points 1 to 9 indicate the load when the X-ray images were taken.

III. Results and Discussion

A. Progression of damage and failure from X-ray μCT

Two dimensional (2D) tomographic slices of the specimen were first generated from X-ray projection images (sinograms) using a commercial reconstruction algorithm (Octopus v8). Data were processed using image processing tools and visualized in AMIRA 6.2 (FEI, Inc.). The solid materials (matrix and fiber) and vacancies (cracks, voids and air) had a different gray-scale intensity representation. By segmenting the appropriate grey-scale values, cracks on the specimen can be defined as shown in Figure 6. The multiple damage progression was analyzed in two-dimensional tomographic slice image. The transverse matrix cracks on 90° plies were observed in the yz-plane images. Comparing with the laboratory X-ray source, the fiber, matrix and crack were clearly distinguished owing to the high power of the synchrotron beam and a finer resolution.

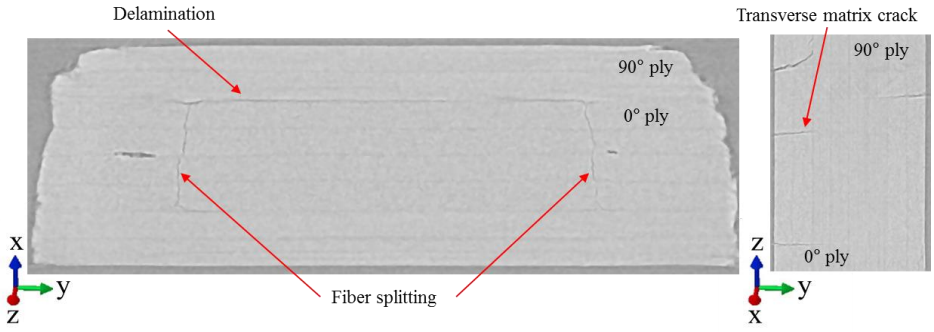

Figure 6: Example of 2D tomographic slice images obtained from the in situ test on the SENT specimen

Computational tomography (CT) reconstruction allows the volume of a given sample to be visualized in a three-dimensional grey-scale map in which the grey-scale value correlates to the local material X-ray adsorption coefficient, depending on atomic number. 3D tomography images of the specimen undergoing mechanical loading were reconstructed from sets of X-ray projection images (radiographs) recorded as the test instrument was rotated stepwise through an angular range of 180 degrees. Figure 7 shows internal cracks displayed in the fully 3D tomography when the applied loads were at 35%, 45%, 57% and 68% of the failure load. Through the series of the tomography images, the entire progress of different failure modes was observed. Transverse matrix cracks in the 90° plies and the fiber directional splitting in the 0° plies occurred first near the notch tip as shown in Figure 7 (a). More failure patterns were found as the load increased as shown in Figure 7 (b), (c) and (d). As clearly depicted in Figure 7, the damage propagation pattern was dependent on the local microstructure of the laminated composite, i.e., transverse cracks in the 90° layers and fiber splitting in 0° layers. Delamination was also observed in the opposite side of the initial notch. As the load was increased, the transverse matrix cracks, spitting and delamination became

deeper and longer. The new transverse matrix cracks (yellow color in Figure 7 (c) and (d)) were initiated in the 90° plies almost symmetrically with respect to the central plane at the notch tip. The distances of transverse matrix cracks were measured and they are shown in Figure 7 (d). Figure 8 shows the same specimen in Figure 21, but from a different viewpoint. In order to clearly observe the fiber splitting mode, the 3D tomography images were viewed in the xy-plane at the same loading steps used in Figure 8.

Through the tomography images such as Figure 7 and Figure 8, the multiple failure modes were quantified in terms of the crack density as the applied load increased. Densities of each crack segment were separately calculated and quantified in the crack volume divided by specimen volume. The crack volume was calculated by multiplying the voxel size to the number of voxels in the crack. The length and depth of a crack were calculated by multiplying the pixel size and the number of pixels in the crack. In the present experiment setting, the volume of the voxel was 0.091125 μm^3 since the pixel size was 0.45 μm. Various transverse matrix cracks observed at different applied loads are denoted as trans_number in Figure 9 (a). The densities of the initial transverse matrix cracks were increased as the applied load was increased as shown in Figure 9 (b). Additional transverse matrix cracks were initiated at 57% of the ultimate tensile stress and the corresponding densities rapidly grew. When the new cracks were propagated, the growth of the previous cracks were slowed down. The fiber directional splitting and delamination were constantly increased as the applied load was increased as shown in Figure 9 (c).

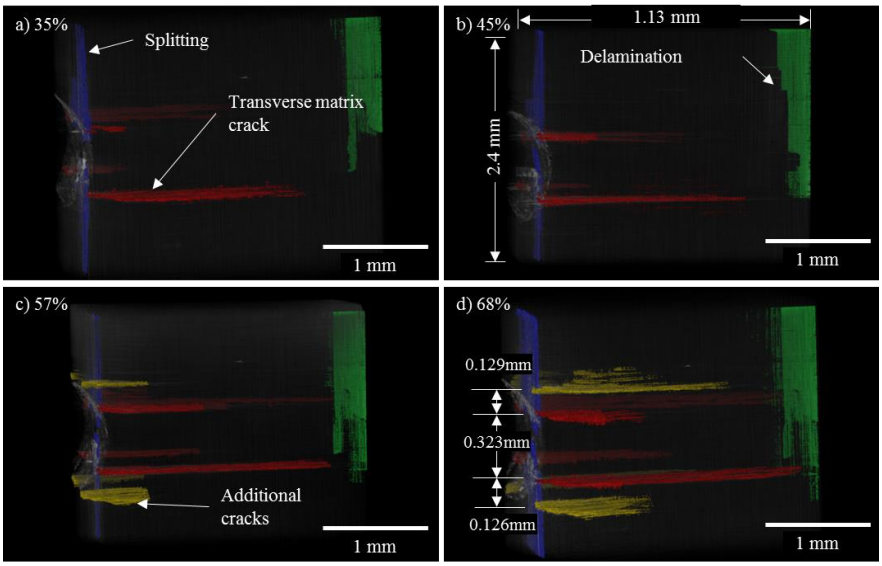

Figure 7: Fully 3D computed tomography result of in situ tensile test on the SENT specimen

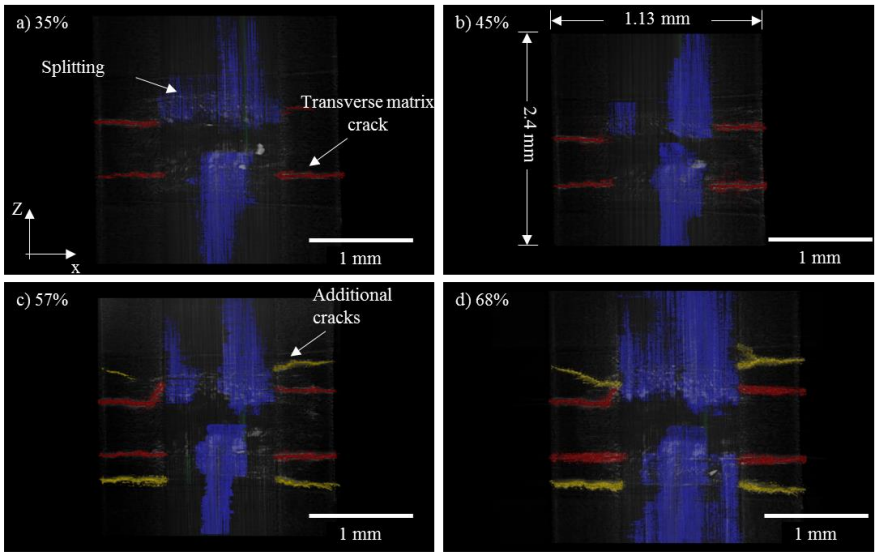

Figure 8: 3D tomography images for the SENT specimen viewed in the xy-plane

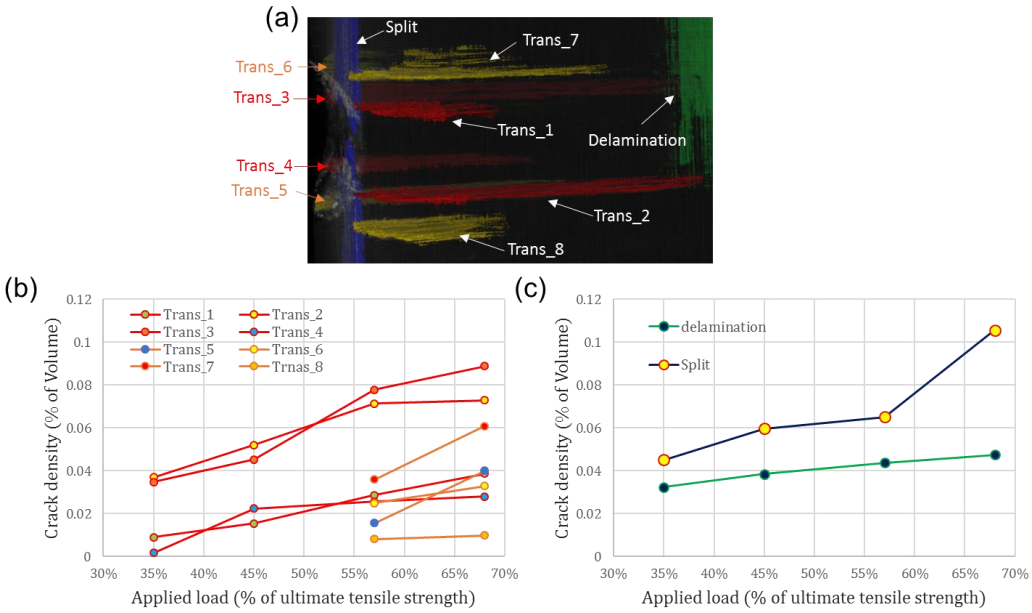

Figure 9: (a) Denotation of each crack (b) Growth of the densities of various transverse matrix cracks (c) Densities of delamination and splitting failure

B. Digital volume correlation technique

For the quantitative deformation analysis of the composite specimen, a digital volume correlation (DVC) technique in conjunction with synchrotron X-ray micro-computed tomography is proposed. As mentioned above, digital image correlation (DIC) technique is now widely used to investigate the progressive damage and failure response of composite materials, but the information obtained from DIC is limited to surfaces where speckle patterns are applied. For the needs on the quantification of subsurface material, DIC has been extended to 3D domain as a name of DVC by conjunction with micro computed tomography (μCT). The DVC technique can be considered as a straightforward extension of the well-established digital image correlation (DIC) and shares its simplicity in principles and effectiveness in applications [10-12]. DVC technique computes 3D full-field displacement data by tracking natural textures in 3D volume images, sequentially taken while a specimen is being deformed. Volume data are discretized with cubical grids (subvolumes), and DVC algorithm tracks the new positions of each subvolume in the next volume image using a template matching method. From its starts on implementation on medicine and biology, nowadays it has been extensively applied in the characterization of various materials including bones [10, 13], soft materials [14, 15], wood [16], sand [17], and ceramic [18]. Through the development on μCT technique, the resolution of obtained data is over 1 micron with the better image quality of smaller level noise and less artefact, which means quantification of subsurface deformation in micro-length scale is now available by conjunction with DVC technique. However, compared with DIC, the computational burden of DVC is much heavier due to its additional degree of freedom (DOF). Thus, high computation speed of DVC has become one of main issues in this area that challenges researchers in the past decade [12]. For efficient and fast tracking from massive high-resolution volume data, the present DVC algorithm implements a simplified matching process based on the zero-normalized cross correlation (ZNCC) method and parallel-computing scheme is also applied to achieve computational efficiency.

The presenting DVC algorithm correlates reference and target subvolumes with a fully 3D-based ZNCC method. Figure 10 shows several stacks of 2D tomograms in a reference state and a deformed state and they are equivalent to the 3D volume of each state. DVC process starts from defining points of interest (POIs) in the 3D space of volume of interest (VOI) on the same global coordinates in both reference and deformed states. Then a subvolume with its center conforming to a POI is constructed in the 3D volume of reference state. Eq. (1) computese a correlation coefficient value in 3D space by including all the pixels inside a subvolume as shown in Figure 10.

$$C_{IJK} = \frac{\sum_{i=m}^{M}\sum_{j=1}^{N}\sum_{k=1}^{L}\left(f\left(x_i,y_j,z_k\right)-f_m\right)\left(g\left(x_i',y_j',z_k'\right)-g_m\right)}{\sqrt{\sum_{i=1}^{M}\sum_{j=1}^{N}\sum_{k=1}^{L}\left(f\left(x_i,y_j,z_k\right)-f_m\right)^2}\sqrt{\sum_{i=1}^{M}\sum_{j=1}^{N}\sum_{k=1}^{L}\left(g\left(x_i',y_j',z_k'\right)-g_m\right)^2}} \tag{1}$$

$$C_{ZNCC}(P) = \frac{\sum_{x=-M}^{M}\sum_{y=-M}^{M}\sum_{z=-M}^{M}\left(f\left(x,y,z\right)-f_m\right)\left(g\left(x',y',z'\right)-g_m\right)}{\sqrt{\sum_{x=-M}^{M}\sum_{y=-M}^{M}\sum_{z=-M}^{M}\left(f\left(x,y,z\right)-f_m\right)^2}\sqrt{\sum_{x=-M}^{M}\sum_{y=-M}^{M}\sum_{z=-M}^{M}\left(g\left(x',y',z'\right)-g_m\right)^2}} \tag{1}$$

where C_{ZNCC} is a correlation coefficient, P is a vector defined between the two center points of the reference and the target subvolumes as shown in Figure 10, M is the half-width of the cubical subvolume, $f(x, y, z)$ is a grayscale intensity at coordinates of (x, y, z) in the reference subvolume, and $g(x', y', z')$ is the intensity value at (x', y', z') in the target subvolume. f_m and g_m are the mean intensity values of every pixel inside the subvolume in the reference and deformed states, respectively.

where C_{IJK} is a correlation coefficient, I, J and K are the pixel numbers in which the comparing subvolume can move in the search area in x, y and z directions, respectively, and f_m and g_m are the mean intensity values of all the pixels inside the subvolumes in the reference and deformed states.

The correlation coefficients, C_{ZNCC}, have a practical range of 0 to 1 where 1 means two facets in the reference and deformed states are perfectly correlated. Physical meaning of Eq. (1) can be explained by considering two comparing images (subvolumes) as two vectors. The ZNCC equation is then regarded as the inner product of two vectors divided by the norms of each vector, which is equivalent to the cosine of the angle between the two vectors. Therefore, two vectors representing the reference and the target subvolumes are the same when the angle is zero, resulting in the correlation coefficient value of one.

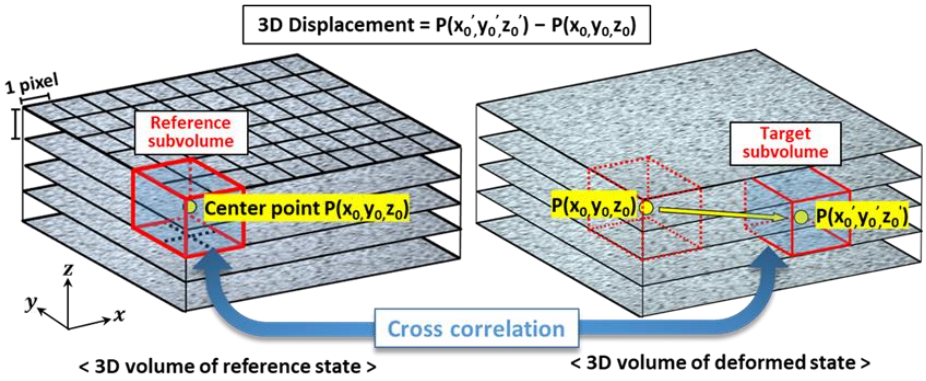

Figure 10: Subvolumes and the correlation process of the present DVC algorithm

The present DVC algorithm is applied to the quantitative deformation analysis of a composite material subjected to a tensile load. Carbon fiber/epoxy prepregs material was utilized to manufacture the laminated composite specimen with the layup sequence of $[90_2/0_2]_S$. Detailed dimensions of the specimen are shown in Figure 11. The specimen was imaged through a laboratory scale X-ray μCT device (Zeiss Xradia Versa 520) in Korea Institute of Science and Technology (KIST) while the specimen was loaded in the Deben microtest tensile stage. Tomograms were taken at several loading sequences; 250N, 500N, 750N and 1000N. At each loading step, total 980 slice-images (tomograms) were obtained with the resolution of 986×1006 pixels per image. The length of one pixel is correspondent to 4.26 μm. A sample slice-image is shown on the right side of Figure 11. For the deformation analysis on the loaded specimen, the tomograms are cropped so that the volume of interest is properly defined inside the material as shown in Figure 11. As a result, the size of the VOI in the *xy*-plane where the present DVC algorithm is applied is set to 400×240 pixels (1.7×1 mm) as indicated in Figure 11.

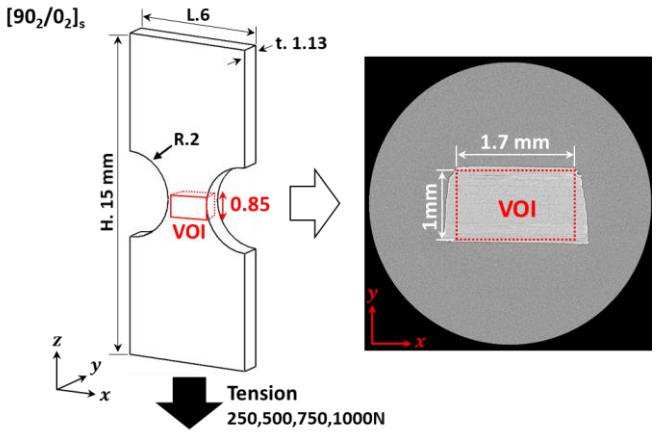

Figure 11: Specimen configuration (left) and a sample tomogram with the volume of interest (right)

Figure 12 shows the 3D-rendered results of tomography images with various failure patterns in different colors. As can be seen in Figure 12, the X-ray μCT is capable of visualizing the progression of failure occurring inside the material. At the load of 500 N, fiber splitting failure in 0-degree layers (blue color) is detected while only transverse cracks in 90-degree layers (red color) are observed at 250 N. Additional transverse cracks (yellow color) are also found as the load is increased from 250 N to 500 N. The present DVC algorithm is applied between the initial transverse crack as indicated in Figure 12, resulting in the length of the VOI being 0.85 mm along the *z*-direction.

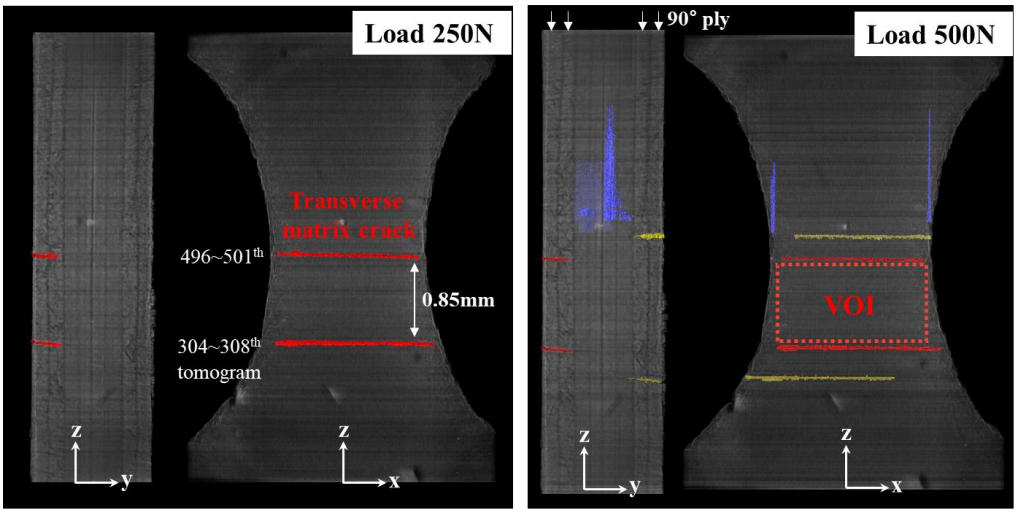

Figure 12: Visualization of cracks in 3D-rendered images at 250 N (left) and 500 N (right)

The VOI region is discretized with total 3588 cubical subvolumes while the size of one subvolume is 31×31×31 voxels. The subvolumes are evenly distributed over the region and each subvolume is overlapped with adjacent ones by 15 voxels in the *x*, *y* and *z* directions. Tomography images at 250 N and 500 N are used for the deformation analysis using the present DVC algorithm. Figure 13 shows the obtained displacement field between 250 and 500 N loading steps. The displacement fields are mapped on the un-deformed configuration.

As shown in Figure 13, the present DVC method produces a reasonable displacement result. From the present DVC analysis, it is found that the inner section (0° plies) of the specimen deforms more than outer 90° plies. As shown in Figure 12, since the transverse cracks are already present in the 90° plies at the load of 250 N, the 0° plies in the VOI carries almost all the load as the load increase from 250 N to 500 N. As a result, the deformation of the 0° layers should be a bit larger than that of the 90° layers. As can be seen in Figure 13, the present DVC is capable of capturing this deformation behavior and it can be concluded that all the subvolumes are appropriately correlated without any outliers.

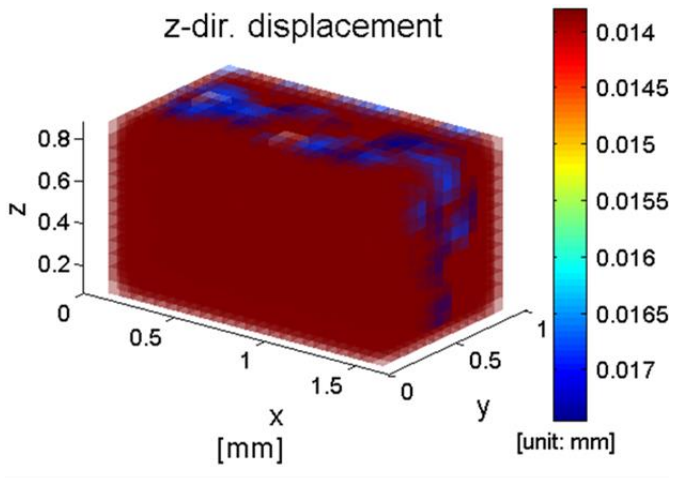

Figure 13: Displacement field between 250 and 500 N obtained from the present DVC algorithm

IV. Conclusion

In situ mechanical test results on the single edge notched specimen with the layup sequence of $[90_2/0_2]_S$. have been presented. Custom-built loading frame is designed and fabricated to perform the in situ tests. The loading frame is designed such that it can be mounted on the test stage at the synchrotron facility and X-ray images can be taken at certain loading steps. Reconstructed 3D tomography images clearly visualize multiple failure modes occurring at the different loading steps. Interactive failure mechanisms inside the heterogeneous composite material is quantified using densities of each failure mode computed from image processing. DVC technique combined with the X-ray μCT technology is applied to examine the mechanical behavior inside of a laminated composite material. It is shown that the natural texture of the composite material can be used in the DVC approach and the present DVC algorithm can track realistic motions of each subvolume without any outliers.

Acknowledgments

The authors are grateful for the financial support through the Lockheed Martin's Republic of Korea Science, Technology and Research (RoKST&R) program in the year of 2015.

References

[1]Buffiere, J. Y., et al. (2010). "In Situ Experiments with X ray Tomography: an Attractive Tool for Experimental Mechanics," Experimental Mechanics 50(3): 289-305.

[2]Moffat, A. J., et al. (2010). "In situ synchrotron computed laminography of damage in carbon fibre-epoxy [90/0] s laminates," Scripta Materialia 62(2): 97-100.

[3]Wright, P., et al. (2010). "High resolution tomographic imaging and modelling of notch tip damage in a laminated composite," Composites Science and Technology 70(10): 1444-1452.

[4]Scott, A. E., et al. (2011). "In situ fibre fracture measurement in carbon-epoxy laminates using high resolution computed tomography," Composites Science and Technology 71(12): 1471-1477.

[5]Garcea, S. C., et al. (2014). "Fatigue micromechanism characterisation in carbon fibre reinforced polymers using synchrotron radiation computed tomography," Composites Science and Technology 99: 23-30.

[6]Hufenbach, W., et al. (2012). "A test device for damage characterisation of composites based on in situ computed tomography," Composites Science and Technology 72(12): 1361-1367.

[7]Bale, H. A., et al. (2013). "Real-time quantitative imaging of failure events in materials under load at temperatures above 1,600 degrees C," Nature Materials 12(1): 40-46.

[8]Sket, F., et al. (2015). "In situ tomographic investigation of damage development in +/- 45 degrees carbon fibre reinforced laminates," Materials Science and Technology 31(5): 587-593.

[9]PAL website, http://pal.postech.ac.kr/paleng/bl/6C

[10]Bay, B. K., Smith, T. S., Fyhrie, D. P., & Saad, M. (1999). Digital volume correlation: three-dimensional strain mapping using X-ray tomography. Experimental mechanics, 39(3), 217-226.

[11]Schreier, H., Orteu, J. J., & Sutton, M. A. (2009). Image correlation for shape, motion and deformation measurements. Springer US.

[12]Wang, T., Jiang, Z., Kemao, Q., Lin, F., & Soon, S. H. (2016). GPU accelerated digital volume correlation. Experimental Mechanics, 56(2), 297-309.
[13]Zauel, R., Yeni, Y. N., Bay, B. K., Dong, X. N., & Fyhrie, D. P. (2006). Comparison of the linear finite element prediction of deformation and strain of human cancellous bone to 3D digital volume correlation measurements. Journal of biomechanical engineering, 128(1), 1-6.
[14]Franck, C., Hong, S., Maskarinec, S. A., Tirrell, D. A., & Ravichandran, G. (2007). Three-dimensional full-field measurements of large deformations in soft materials using confocal microscopy and digital volume correlation. Experimental Mechanics, 47(3), 427-438.
[15]Huang, J., Pan, X., Li, S., Peng, X., Xiong, C., & Fang, J. (2011). A digital volume correlation technique for 3-D deformation measurements of soft gels. International Journal of Applied Mechanics, 3(02), 335-354.
[16]Forsberg, F., Sjödahl, M., Mooser, R., Hack, E., & Wyss, P. (2010). Full Three-dimensional strain measurements on wood exposed to three-point bending: analysis by use of digital volume correlation applied to synchrotron radiation micro-computed tomography image data. Strain, 46(1), 47-60.
[17]Hall, S. A., Bornert, M., Desrues, J., Pannier, Y., Lenoir, N., Viggiani, G., & Bésuelle, P. (2010). Discrete and continuum analysis of localised deformation in sand using X-ray μCT and volumetric digital image correlation. Géotechnique, 60(5), 315-322.
[18]Marrow, J., Reinhard, C., Vertyagina, Y., Saucedo-Mora, L., Collins, D., & Mostafavi, M. (2014). 3D studies of damage by combined X-ray tomography and digital volume correlation. Procedia Materials Science, 3, 1554-1559.